Chinese Journal of Catalysis 34 (2013) 593–603

available at www.sciencedirect.com

ScienceDirect

journal homepage: www.elsevier.com/locate/chnjc

Article

Study of crystallization process of SAPO-11 molecular sieve

LI Bing [a], TIAN Peng [a], QI Yue [a], ZHANG Lin [a], XU Shutao [a], SU Xiong [a,b], FAN Dong [a,b], LIU Zhongmin [a,*]

[a] *Dalian National Laboratory for Clean Energy, National Engineering Laboratory for Methanol-to-Olefins, Dalian Institute of Chemical Physics, Chinese Academy of Sciences, Dalian 116023, Liaoning, China*

[b] *University of Chinese Academy of Sciences, Beijing 100049, China*

ARTICLE INFO

Article history:
Received 21 November 2012
Accepted 30 December 2012
Published 20 March 2013

Keywords:
SAPO-11 molecular sieve
Characterization
Crystallization process
Silicon distribution

ABSTRACT

The crystallization process of SAPO-11 was studied using a combination of X-ray diffraction, scanning electron microscopy, X-ray fluorescence, nuclear magnetic resonance, and X-ray photoelectron spectroscopy. In the initial stage of crystallization, SAPO-11 was formed along with an unknown crystalline material composed of Si–P–Al. As crystallization evolved, the crystalline material dissolved. The SAPO-11 formation rate increased greatly, which is characteristic of fast crystallization. After 2.33 h, the relative crystallinity of SAPO-11 reached ~100% and remained at a high level until crystallization was complete. Si was incorporated into the SAPO-11 framework from the initial stage of crystallization. The Si content of the solid samples increased with crystallization time. Most of the Si atoms existed as Si islands in the SAPO-11 framework, resulting in the presence of multiple coordination environments, i.e., Si(*n*Al, (4 – *n*)Si), *n* = 0–4. X-ray photoelectron spectroscopy analysis revealed Si enrichment on the external surfaces of the SAPO-11 crystals. Based on the experimental results, the distribution of Si in the crystals is not uniform, showing an increasing trend from the core to the surface.

1. Introduction

The first synthesis of silicoaluminophosphate molecular sieves (SAPO-*n*) was reported by the Union Carbide Corporation in the 1980s [1]. SAPO-11 is one of the most important members of the SAPO family. It consists of elliptical, one-dimensional, 10-membered-ring channels with a pore opening of 0.40 nm × 0.65 nm [2]. SAPO-11 molecular sieve has outstanding thermal and hydrothermal stabilities, and has played an important role in petrochemical processes, such as isomerization, catalytic cracking, hydrocracking, and isodewaxing [3,4]. It is worth pointing out that SAPO-11 exhibits excellent catalytic reactivity in the isodewaxing of lubricant oils, which is already used in industry [5].

SAPO-11 molecular sieve is mainly synthesized using hydrothermal methods, and detailed studies of SAPO-11 synthesis have been carried out by many researchers. Wang et al. [6] investigated the effects of the Si source, Si content, amount of template, and crystallization conditions (temperature, time and pH) on SAPO-11 synthesis. They found that the Si source is one of the main factors affecting the synthesis and structure of SAPO-11. Liu et al. [7] used di-*n*-propylamine (DPA), diisopropylamine, or a mixture of these as templates for synthesizing SAPO-11. They found that the impurities that appeared in the synthesis using a single template can be effectively avoided by using a dual-template method. Liu et al. [8] studied the effect of the synthesis conditions on the distribution of Si in the framework of SAPO-11 molecular sieve. Prolonging the crystallization time, raising the temperature, lowing the Si/Al ratio, and controlling the pH of the initial gels promote uniform distribution of Si in the framework. They obtained SAPO-11 molecular sieve with highly dispersed Si. Zhang et al. [9] investigated the

* Corresponding author. Tel/Fax: +86-411-84379335; E-mail: liuzm@dicp.ac.cn
DOI: 10.1016/S1872-2067(12)60542-7 | http://www.sciencedirect.com/science/journal/18722067 | Chin. J. Catal.,Vol. 34, No. 3, March 2013

synthesis and characterization of SAPO-11 molecular sieve in the presence of hydrofluoric acid (HF). Compared with the synthesis in the absence of HF, adding HF increases the crystallization rate and crystallinity of SAPO-11 molecular sieve. Microwave synthesis [10], solvothermal synthesis [11], and dry-gel methods [12,13] have also been reported for the synthesis of SAPO-11 molecular sieve.

Huang et al. [12] used solid-state nuclear magnetic resonance (NMR) spectroscopy and other methods to study the crystallization process of AlPO-11 synthesized by dry-gel conversion. They found that the initial amorphous material is first converted to a semicrystalline intermediate with 10-membered-ring channels. As the crystallization proceeds, the intermediate is transformed into AlPO-11. They also used ^{17}O NMR spectroscopy to investigate the effect of water on the AlPO-11 crystallization process during dry-gel conversion. Direct evidence of the involvement of water in molecular sieve crystallization was obtained [14]. Zhang et al. [15] studied the influence of water content on the hydrothermal crystallization of AlPO-11, using ultraviolet (UV), Raman, X-ray diffraction (XRD), and NMR characterization methods. They proposed possible intermediate fragments in the crystallization process of AlPO-11, based on a combination of their experimental results and theoretical computations [16]. So far, there have been few detailed studies of the crystallization process of SAPO-11. The crystallization process of SAPO-11 might be different from that of AlPO-11 because of the presence of Si. However, it is very important to determine the status and distribution of Si in SAPO-11 with increasing crystallization time because the incorporation of Si into the molecular sieve framework generates acidic centers with catalytic properties. Studies of the crystallization process of SAPO-11 can improve understanding of the crystallization mechanism. They will also be helpful in effectively controlling SAPO-11 synthesis.

In this paper, SAPO-11 molecular sieve was synthesized using a hydrothermal method in a 2-L autoclave with a sampling pipeline. The samples obtained at different times were characterized by XRD, X-ray fluorescence spectroscopy (XRF), scanning electron microscopy (SEM), magic-angle spinning (MAS) NMR, and X-ray photoelectron spectroscopy (XPS) methods. Some new insights into the crystallization process of SAPO-11 molecular sieves were obtained.

2. Experimental

2.1. Preparation of SAPO-11 molecular sieve

In all syntheses, pseudoboehmite (Al_2O_3, 67 wt%), silica sol (SiO_2, 27.5 wt%), and phosphoric acid (85 wt%) were used as sources of Al, Si, and P, respectively. The template was DPA (chemically pure). The initial gel was prepared by mixing all the raw materials in a molar composition of 1.1 DPA:0.4 SiO_2:0.86 Al_2O_3:1 P_2O_5:55 H_2O. The mixture was transferred into a 2-L stainless-steel autoclave, and the autoclave was sealed. The temperature was gradually raised to 200 °C, with continuous stirring, and kept stable for crystallization. The crystallization time was recorded from the start of heating. Liquid samples were removed at different times. At sampling times of 0.75 and 1.22 h, the corresponding temperatures were 100 and 150 °C, respectively. After 1.83 h, the temperature reached 200 °C and was then kept constant. The liquid samples were cooled to room temperature. The liquid phase was separated from the solids by centrifugation. The solid materials were washed with water and then dried at 120 °C.

2.2. Preparation of other SAPO molecular sieves

Triethylamine (TEA) was used as a template for the synthesis of SAPO-5. The initial gel composition was 1.2 TEA:0.4 SiO_2:1 Al_2O_3:1 P_2O_5:60 H_2O. SAPO-5 was crystallized at 200 °C for 17 h.

In a similar procedure, SAPO-34 was synthesized using TEA as the template. The initial gel composition was 3.5 TEA:0.3 SiO_2:1 Al_2O_3:1 P_2O_5:55 H_2O. SAPO-34 was crystallized at 200 °C for 48 h. The sample was labeled SAPO-34-TEA.

SAPO-35 was synthesized using hexamethyleneimine (HMI) as the template. The initial gel composition was 1.33 HMI:0.5 SiO_2:1 Al_2O_3:0.96 P_2O_5:55 H_2O. SAPO-35 was crystallized at 200 °C for 24 h.

2.3. Characterization

Powder XRD patterns were recorded on a PANalytical X'Pert PRO X-ray diffractometer, using Cu K_α (λ = 0.15418 nm) radiation at 40 kV and 40 mA. Element analysis was performed using a Philips Magix 2424X XRF spectrometer. The morphologies of samples were examined by SEM, using a KYKY-AMRAY-1000B instrument (CAS Scientific Instrument Company). Solid-state NMR spectra were recorded on a Bruker AvanceIII 600 spectrometer. The resonance frequencies of ^{29}Si, ^{27}Al, and ^{31}P were 119.2, 156.4, and 242.9 MHz, respectively. ^{29}Si MAS NMR spectra were acquired using a 7-mm probe with proton decoupling; 2.5 μs, corresponding to a $\pi/4$ pulse length, was applied, with a 10-s delay and a rotor spinning rate of 5 kHz. 4,4-Dimethyl-4-silapentane-1-sulfonic acid was used as the chemical shift reference. ^{27}Al MAS NMR spectra were recorded using a 4-mm probe with a $\pi/8$ pulse length of 0.75 μs, a 2-s delay, and a rotor spinning rate of 13 kHz. $NH_4Al(SO_4)_2{\cdot}12H_2O$ was used as a secondary chemical shift reference (δ_{Al} = −0.4). ^{31}P MAS NMR spectra were measured using a 4-mm probe with high-power proton decoupling at a spinning speed of 10 kHz. A $\pi/4$ pulse strength of 2.25 μs was used with a delay of 4 s. The chemical shift of ^{31}P was referenced to 85% phosphoric acid aqueous solution. XPS measurements were performed using a Thermo ESCALAB 250Xi spectrometer with Al K_α radiation as the excitation source. The surface charge of the sample was calibrated by referencing to the Al 2*p* peak of Al_2O_3 at 74.7 eV.

3. Results and discussion

3.1. XRD

Figure 1 shows the XRD patterns of as-synthesized samples with different crystallization time. In the initial crystallization

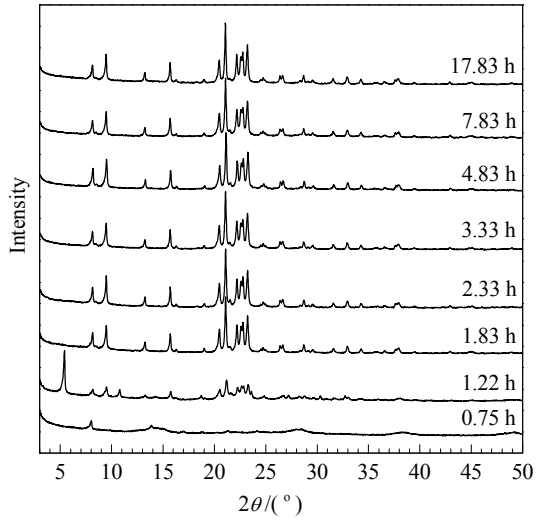

Fig. 1. XRD patterns of as-synthesized samples with different crystallization time.

stage (0.75 h), the solid sample was mainly composed of amorphous boehmite because of the short crystallization time and low temperature [17]. However, a weak peak at 8° can be found in the XRD pattern, indicating the appearance of a small amount of crystalline material in the system. After 1.22 h, the typical diffraction peaks of SAPO-11 molecular sieve, at 8.1°, 9.5°, 13.2°, 15.7°, and 21°, were detected, implying formation of the SAPO-11 crystalline phase. There were two obvious peaks, at 5.4° and 10.8°, which were not diffraction peaks of SAPO-11. Based on the peak positions, these might be from a layered crystalline phase. These two peaks disappeared after the temperature reached 200 °C (t = 1.83 h). Pure SAPO-11 molecular sieve was then obtained.

Based on an intensity summary of the six strongest peaks in the XRD patterns of SAPO-11, the relative crystallinity of the sample at different crystallization times was calculated (the crystallinity of the sample at 17.83 h was defined as 100%). The crystallization curve for SAPO-11 is shown in Fig. 2. Before 2.33 h, the relative crystallinity increased sharply with increasing crystallization time. At 1.83 h, the relative crystallinity of the sample reached 81%. This is close to 100%, the value at a crystallization time of 2.33 h. The relative crystallinity later fluctuated within a certain range (> 90%). These results indicated fast crystallization of SAPO-11 molecular sieve.

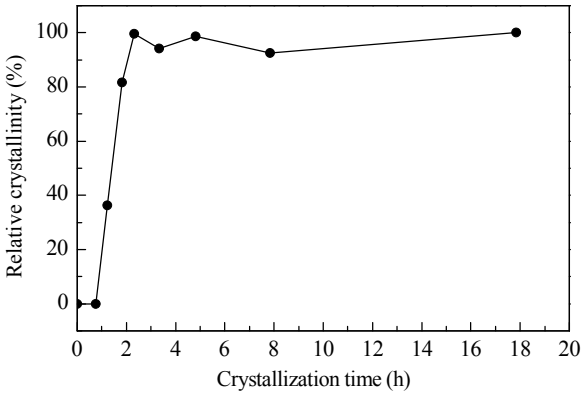

Fig. 2. Crystallization curve of SAPO-11.

3.2. SEM

Figure 3 shows the SEM images of as-synthesized samples with different crystallization times. At 0.75 h, only amorphous material appeared in the solid sample. For a crystallization time of 1.22 h, some spherical aggregates of SAPO-11 were observed. In addition, there was a small amount of strip crystals. As the crystallization time increased, the amount of amorphous materials gradually decreased. At 1.83 h, the strip crystals totally disappeared, and the amount of spherical aggregation increased significantly. The morphology of the solid sample then remained almost unchanged with time.

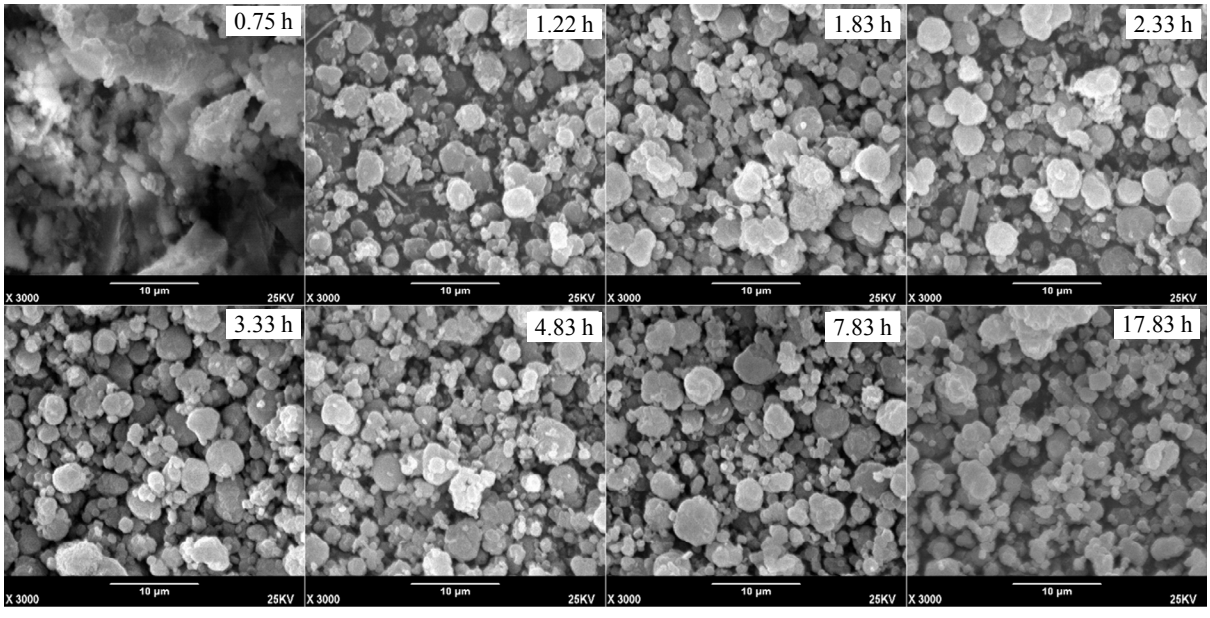

Fig. 3. SEM images of as-synthesized samples with different crystallization time.

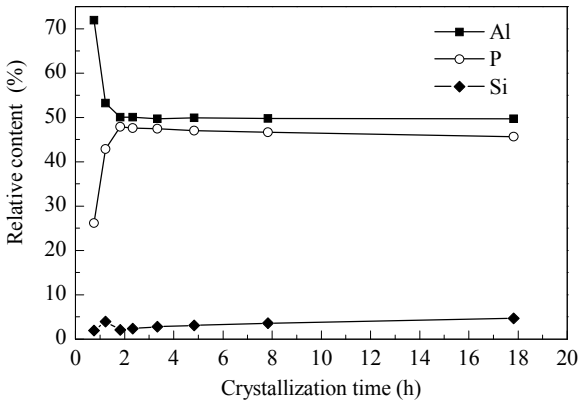

Fig. 4. Chemical compositions of as-synthesized samples with different crystallization time.

3.3. XRF

The chemical compositions of the as-synthesized samples were obtained using XRF. Figure 4 shows the changes in the relative molar contents of P, Al, and Si in the solid samples at different crystallization time. In the initial stage of crystallization (before 1.83 h), the P content of the solid samples increased significantly (from 26.14% at 0.75 h to 47.89% at 1.83 h), but that of Al decreased rapidly (from 71.9% at 0.75 h to 50.05% at 1.83 h). This indicates that Al species from the raw materials continued to dissolve into the liquid phase with time, and the amorphous materials observed by SEM in the early crystallization period should be mainly from unreacted alumina. As the crystallization time increased, the Al content of the solid samples was stable at 50%, the P content showed a weak downward trend, and the content of Si increased correspondingly. The sum of the numbers of moles of Si and P remained around 50%, close to that of Al. It is worth noting that the Si content of the sample at 1.22 h showed a maximum value. In addition, comparing the sample at 1.83 h with the final product shows that the change in the relative molar content of Si was larger than those of P and Al. The content of Si in the sample at 1.83 h was 2.06%. This increased 1.26-fold to 4.66% at 17.83 h.

3.4. Crystallization solution pH

The pH of the crystallization solution is closely related to the status of all the raw materials under the synthesis conditions. Before 2.33 h, the pH of the crystallization solution increased significantly with increasing crystallization time (shown in Fig. 5). After that, there were only small changes in the pH. Considering the above results, we concluded that the rapid increase in the pH of the solution during the initial crystallization period, up to 2.33 h, was caused by consumption of phosphoric acid and aluminum oxide in the reaction. Correspondingly, a large amount of molecular sieves were synthesized. In addition, as the P content of the solution decreased, the organic amine that combined with phosphoric acid in the initial stage was gradually released, which also resulted in an increase in the pH. After 2.33 h, the pH of the crystallization solution remained almost unchanged.

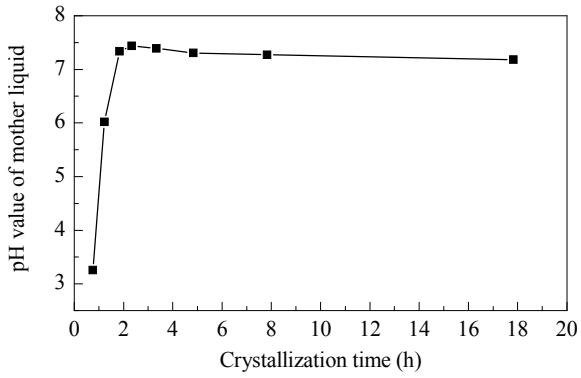

Fig. 5. pH values of crystallization solutions at different crystallization time.

3.5. Solid-state MAS NMR

^{31}P and ^{27}Al MAS NMR spectra of the as-synthesized samples at different crystallization time are shown in Fig. 6 respectively. Only one broad peak, at δ = −16, is observed in the ^{31}P MAS NMR spectrum of the sample at 0.75 h. This peak can be assigned to $P(OH)_x[OAl_{(tet)}]_y[OAl_{(oct)}]_{4-(x+y)}$ (x = 1, 2) species in the amorphous aluminophosphate phase [18]. Correspondingly, there are two resonance peaks in the ^{27}Al MAS NMR spectrum of the sample, which are related to five-coordinated (δ = 8) and six-coordinated (δ = −12) Al species in the amorphous Al

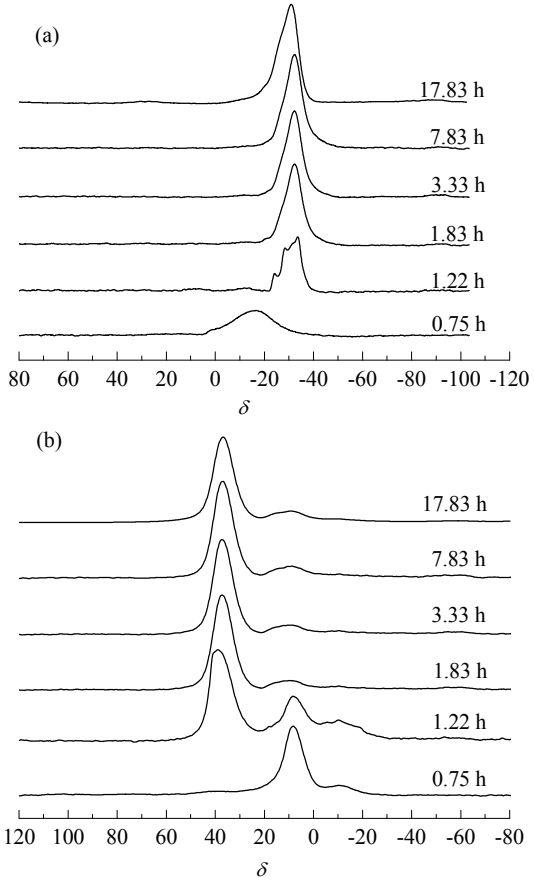

Fig. 6. ^{31}P MAS NMR (a) and ^{27}Al MAS NMR (b) spectra of as-synthesized samples.

source and amorphous aluminophosphate, respectively [11,19,20]. After 1.22 h, the broad peak in the ^{31}P MAS NMR spectrum almost disappeared, indicating that there was a smaller amount of amorphous aluminophosphate left in the sample. At the same time, several relatively sharp peaks at δ = −24, −28.4, and −33.6 appeared in the spectrum, arising from highly crystalline four-coordinated P species in the aluminophosphate [12,18]. This demonstrates that the P species in the solid samples were highly condensed and the P atoms had complex coordination environments. In addition, obvious changes can be observed in the ^{27}Al MAS NMR spectrum. A strong asymmetric resonance appeared at δ = 38.8. The intensity of the peak at δ = 8 became weak. Generally, the chemical shifts of tetrahedral Al species in microporous aluminophosphate materials are in the range δ = 35–48 [21]. The new resonance at δ = 38.8 in the sample at 1.22 h is therefore assigned to four-coordinated Al species. The weakening of the peak at 8 ppm indicates that the content of amorphous Al source in the solid samples was decreasing, which is in agreement with the XRF results. It is worth pointing out that the intensity of the peak at δ = −12, from six-coordinated Al species, did not decrease with dissolution of amorphous aluminophosphate and the Al source, from which it can be deduced that newly formed Al species contribute to the same chemical shift at δ = −12. The ^{31}P and ^{27}Al MAS NMR spectra of the samples were almost unchanged after crystallization for 1.83 h or longer. The resonance at δ = −32 (including the shoulder at δ = −26) in the ^{31}P MAS NMR spectrum is attributed to tetrahedrally coordinated P species in the SAPO-11 framework [12,20]. The peaks at δ = 37 and 8 in the ^{27}Al MAS NMR spectrum are from four-coordinated and five-coordinated Al species in the framework of the molecular sieves [12,17]. These results suggest that the crystallization of SAPO-11 was almost complete, and are consistent with the XDR, SEM, and XRF results.

Comparing the spectra of the samples in the late period of crystallization suggests that the peak at δ = −12 in the ^{27}Al MAS NMR spectrum of the sample at 1.22 h, from octahedral Al species, should be related to the crystalline intermediate phase. As well as tetrahedral Al species (δ = 37) in SAPO-11, the asymmetric resonance at δ = 38.8 in the ^{27}Al MAS NMR spectrum is also attributed to Al species in the intermediate phase. Correspondingly, several peaks in the ^{31}P MAS NMR spectrum are also correlated with the intermediate phase. These results demonstrate that the coordination environments of the Al and P species in the intermediate phase are very complex.

Figure 7(a) presents the ^{29}Si MAS NMR spectra of solid samples at different crystallization times. The spectra of all the samples show a similar broad resonance. Comparing the spectra of the samples at different times, we found that the relative intensity of the peak at δ = −109 in the spectrum of the sample at 1.22 h was higher than those of the other samples. Reports in the literature [2,22–24] show that Si atoms can exist as Si(nAl, (4 − n)Si) (n = 0–4) in the framework of SAPO molecular sieves. As the number of Al atoms around Si decreases, the Si resonance shifts to a higher field (−90 to −110). The peak broadening in the ^{29}Si MAS NMR spectra of the sample at 1.83 h and other highly crystalline samples indicates that there are several

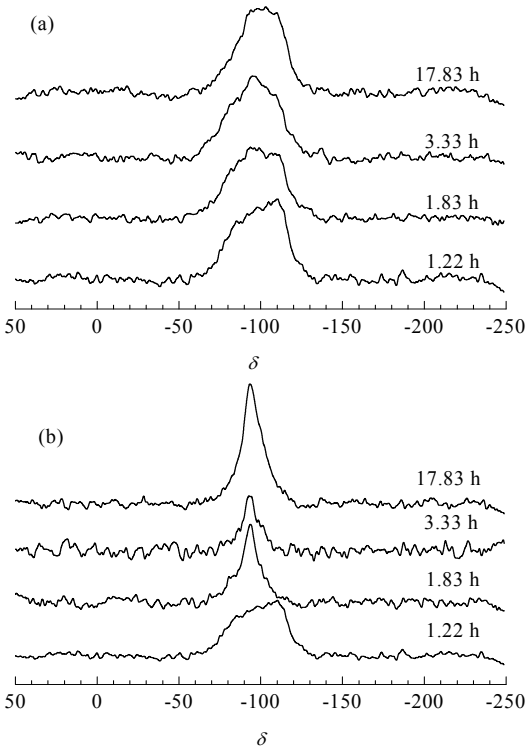

Fig. 7. ^{29}Si MAS NMR (a) and ^{1}H–^{29}Si CP MAS NMR (b) spectra of as-synthesized samples.

types of Si species in the frameworks of the solid samples. Since the sample has two crystal phases in the initial crystallization period (at 1.22 h), as well as a small amount of amorphous materials, it is difficult to assign all the peaks in the ^{29}Si MAS NMR spectrum. Therefore, ^{1}H–^{29}Si cross-polarization (CP) MAS NMR spectra were obtained. The spectra are shown in Fig. 7(b). It is obvious that almost no changes can be observed in the spectrum of the sample at 1.22 h after cross polarization. However, a sharp peak at δ = −93.7 [Si(3Al)] appeared in the ^{29}Si CP MAS NMR spectra of other solid samples, instead of the broad peak seen in the ^{29}Si MAS NMR spectra. The difference between the peak intensity of the sample at 1.22 h and those of the other solid samples in the range −75 to −100 could be correlated with the existence of crystalline intermediates. The assignment of the peak at δ = −110 is still difficult. This peak might arise from the intermediate phase, or it could be related to undissolved raw materials in the liquid phase. Comparing the ^{29}Si MAS NMR and ^{29}Si CP MAS NMR spectra of the solid samples in the later period of crystallization, we infer that the Si atoms exist as Si islands in the molecular sieve framework at this stage. Based on the SM2 (Si substituting P) and SM3 (Si substituting P–Al) mechanisms for incorporation of Si into the SAPO framework, five- and eight-Si islands can be formed in the framework. The structure with five-Si islands contains four Si(3Al, 1Si) and one Si(4Si). The structure with eight-Si islands contains four Si(3Al, 1Si), two Si(2Al, 2Si), and two Si(4Si) [25,26]. The structures with five-Si islands and eight-Si islands both result in the existence of many Si(3Al) species. This is in agreement with the ^{29}Si MAS NMR spectra.

3.6. Analysis of crystallization process

Based on the above results, we consider the crystallization process of SAPO-11 molecular sieves to be as follows.

Significant changes in the initial gel started to occur when heating started. When the crystallization temperature reached 100 °C, most of the P and Si sources had dissolved into the liquid phase. However, the Al source remained in the solid phase as pseudoboehmite. In addition, some amorphous aluminophosphate appeared in the solid samples. When the temperature rose to 150 °C, large amounts of the Al source and amorphous aluminophosphate dissolved into the liquid phase. At the same time, SAPO-11 crystals and an unknown crystalline phase started to appear. The Al content of the solid samples decreased significantly, and the P and Si contents of the solid samples clearly increased. Moreover, the Si content reached a local maximum point. The pH of the solution increased from 3.26 at 100 °C to 6.02 at 150 °C. Theoretically, in the initial crystallization period, with the increase in the pH, it is easy for amorphous silicon oxide to dissolve into the liquid phase. The increase in the Si content of the solid sample should be caused by formation of the intermediate phase, suggesting the existence of Al–P–Si in intermediates. Based on the NMR results, we can deduce that the coordination environments of these atoms in the intermediate phase are more complex than those in SAPO-11. When the crystallization temperature reached 200 °C, amorphous aluminum oxide and the intermediate crystal dissolved completely. A large amount of SAPO-11 started to crystallize, and the relative crystallinity of the sample was 81%. In addition, the solution pH rose to 7.34. The molar content of Si in the sample was only 2.06%. It existed as Si islands in the framework of the SAPO-11 molecular sieve. On extension of the crystallization time to 17.83 h, the coordination environments of Al, Si, and P in the solid sample remained unchanged. The relative molar content of Al was around 50%. The content of P decreased slightly, and that of Si increased to 4.66%. This means that the amount of Si incorporated into the framework increased greatly in the later stages of crystallization.

3.7. Si distribution in SAPO molecular sieve crystals

Based on analysis of the crystallization process, we infer that the distribution of Si in SAPO-11 molecular sieve might be inhomogeneous, and increase from the inside to the surface. This results in a large amount of Si on the external surface of SAPO. To confirm our deduction, XPS was performed on the sample at 17.83 h. The results are listed in Table 1. The results show that the Si/Al ratio on the external surface is around 0.48, which is much higher than the value of 0.09 in the bulk phase, obtained using XRF. This result is in agreement with our previous analysis. This phenomenon could be closely related to changes in the pH of the system. Since the isoelectric point of silicon oxide is at around pH 2, the solution in the initial crystallization stage is acidic, which is not conducive to depolymerization of silicon oxide. The involvement of Si is therefore restricted to formation of the framework. As the crystallization process proceeds and various products are formed, the solution pH rises gradually. Increasing amounts of silicon oxide are depolymerized, resulting in an increase in the number of active Si species in the liquid phase. The amount of Si atoms incorporated into the framework therefore increases significantly, resulting in a large amount of Si on the external surfaces of the molecular sieves.

Table 1
Bulk and surface compositions of SAPO molecular sieves.

Sample	Bulk	Surface
SAPO-11	$Si_{0.045}Al_{0.498}P_{0.458}$	$Si_{0.224}Al_{0.462}P_{0.314}$
SAPO-5	$Si_{0.073}Al_{0.488}P_{0.439}$	$Si_{0.155}Al_{0.420}P_{0.424}$
SAPO-34-TEA	$Si_{0.080}Al_{0.486}P_{0.434}$	$Si_{0.206}Al_{0.453}P_{0.341}$
SAPO-34-DEA *	$Si_{0.164}Al_{0.478}P_{0.358}$	$Si_{0.231}Al_{0.440}P_{0.329}$
SAPO-35	$Si_{0.122}Al_{0.488}P_{0.390}$	$Si_{0.187}Al_{0.478}P_{0.335}$

*Data from Ref. [15]. SAPO-34-DEA was synthesized with diethylamine as template.

According to the literature, it is common for the pH of a synthetic gel to increase as the crystallization of SAPO molecular sieves progresses. We therefore deduced that Si enrichment of the external surface may occur for other SAPO molecular sieves (that is, the Si content of the crystal increases from the core to the shell). So, SAPO-5, SAPO-34, and SAPO-35 molecular sieves were hydrothermally synthesized and characterized by XPS. The results are presented in Table 1. The Si contents on the surfaces of these samples are higher than those in the bulk phase, in agreement with the above speculation. In addition, there are differences among the surface Si contents of the samples. This might be related to the pH of each synthetic solution and the framework structure of the molecular sieves. The phenomenon of Si enrichment on the surface of SAPO molecular sieves has also been reported by other research groups [27,28]. It should be a common characteristic of the crystallization of SAPO molecular sieves.

4. Conclusions

The hydrothermal crystallization process of SAPO-11 molecular sieve was investigated using several characterization methods. In the early stage of crystallization, the Si, P, and Al sources, as well as the amorphous aluminophosphate gel, dissolved into the liquid phase. SAPO-11 was formed along with a crystalline material composed of Si–P–Al. As crystallization continued, the unknown crystalline material dissolved, and SAPO-11 crystallized with fast crystallization characteristics. After heating the gel for 2.33 h, the relative crystallinity of the molecular sieves was close to 100%. This fluctuated within a small range until crystallization was complete. The crystallization process of SAPO-11 followed a solution-mediated transport mechanism, although a solid hydrogel transformation mechanism may also occur in the initial stage of crystallization. Si atoms were incorporated directly into the SAPO-11 framework in the initial stage of crystallization and existed as Si islands. Considering that the content of silicon oxide in the molecular sieves increased gradually with increasing crystallization time, and based on the XPS results, we deduced that the distribution of Si in the SAPO-11 crystal was not uniform. The content of Si increased from the core to the surface of the crys-

Graphical Abstract

Chin. J. Catal., 2013, 34: 593–603 doi: 10.1016/S1872-2067(12)60542-7

Study of crystallization process of SAPO-11 molecular sieve

LI Bing, TIAN Peng, QI Yue, ZHANG Lin, XU Shutao, SU Xiong, FAN Dong, LIU Zhongmin*
Dalian Institute of Chemical Physics, Chinese Academy of Sciences; Graduate University of Chinese Academy of Sciences

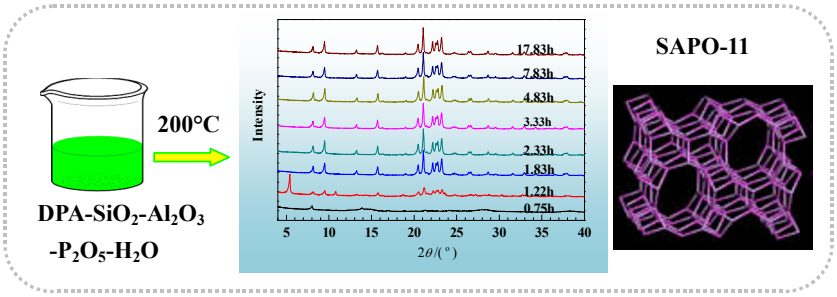

The formation of SAPO-11 exhibited fast crystallization characteristics. The Si content of SAPO-11 increased with time, which led to a non-uniform distribution of Si in the crystals.

tal. In addition, we compared the XPS results of other SAPO molecular sieves. We found enriched Si species on the external surfaces of all the SAPO molecular sieves. We therefore conclude that it is common for the distribution of Si in SAPO molecular sieves synthesized by hydrothermal methods to be non-uniform.

References

[1] Lok B M, Messina C A, Patton R L, Gajek R T, Cannan T R, Flanigen E M. US Patent 4 440 871. 1984
[2] Zhang Sh Zh, Chen Sh L, Dong P, Yuan G M, Xu K Q. *Appl Catal A*, 2007, 332: 46
[3] Luo H J, Wu H J, Wu H Y, Zhang Y Y, Wang Y J. *Ind Catal*, 2011, 19(1): 16
[4] Wang Y J, Li X H, Liu Ch Sh, Jin L L. *Ind Catal*, 2010, 18(3): 1
[5] Tian Zh J, Liang D B, Lin L W. *Chin J Catal*, 2009, 30: 705
[6] Wang Zh M, Yan Z F. *J Fuel Chem Technol*, 2003, 31: 360
[7] Liu Y M, Zhang F M, Shu X T. *Acta Petrol Sin* (*Petrol Proc Sect*), 2002, 18(6): 26
[8] Liu P, Ren J, Sun Y H. *Acta Petrol Sin* (*Petrol Proc Sect*), 2008, 24(4): 388
[9] Zhang Sh Zh, Chen Sh L, Dong P, Jing X J, Jiang K. *Chin J Catal*, 2006, 27: 868
[10] Gharibeh M, Tompsett G A, Conner W C. *Top Catal*, 2008, 49: 157
[11] Sinha A K, Seelan S. *Appl Catal A*, 2004, 270: 245
[12] Chen B H, Huang Y N. *J Phys Chem C*, 2007, 111: 15236
[13] Song Ch M, Feng Y, Ma L L. *Microporous Mesoporous Mater*, 2012, 147: 205
[14] Chen B H, Huang Y N. *J Am Chem Soc*, 2006, 128: 6437
[15] Zhang B, Xu J, Fan F T, Guo Q, Tong X Q, Yan W F, Yu J H, Deng F, Li C, Xu R R. *Microporous Mesoporous Maters*, 2012, 147: 212
[16] Cheng T, Xu J, Li X, Li Y, Zhang B, Yan W F, Yu J H, Sun H, Deng F, Xu R R. *Microporous Mesoporous Mater*, 2012, 152: 190
[17] Liu G Y, Tian P, Zhang Y, Li J Zh, Xu L, Meng Sh H, Liu Zh M. *Microporous Mesoporous Mater*, 2008, 114: 416
[18] Huang Y N, Richer R, Kirby C W. *J Phys Chem B*, 2003, 107: 1326
[19] Zhang L, Bates J, Chen D H, Nie H Y, Huang Y N. *J Phys Chem C*, 2011, 115: 22309
[20] Lutz W, Kurzhals R, Sauerbeck S, Toufar H, Buhl J Chr, Gesing T, Altenburg W, Jäger Chr. *Microporous Mesoporous Mater*, 2010, 132: 31
[21] Yan Zh M, Chen B H, Huang Y N. *Solid State Nucl Magn Reson*, 2009, 35: 49
[22] Borade R B, Clearfield A. *J Mol Catal*, 1994, 88: 249
[23] Wang Sh F, Wang Y J, Gao Y, Zhao X Q. *Chin J Catal*, 2010, 31: 637
[24] Blasco T, Chica A, Corma A, Murphy W J, Agúndez-Rodriguez J, Pérez-Pariente J. *J Catal*, 2006, 242: 153
[25] Barthomeuf D. *J Phys Chem*, 1993, 97: 10092
[26] Shen W L, Li X, Wei Y X, Tian P, Deng F, Han X W, Bao X H. *Microporous Mesoporous Mater*, 2012, 158: 19
[27] Kikhtyanin O V, Toktarev A V, Ayupov A B, Echevsky G V. *Appl Catal A*, 2010, 378: 96
[28] Akolekar D B, Bhargava S K, Gorman J, Paterson P. *Colloids Surf A*, 1999, 146: 375